Rates and Mechanism of Fe(II) Oxidation at Nanomolar Total Iron Concentrations

ARTICLE *in* ENVIRONMENTAL SCIENCE AND TECHNOLOGY · MARCH 1995

Impact Factor: 5.33 · DOI: 10.1021/es00003a033 · Source: PubMed

3 AUTHORS, INCLUDING:

Whitney King
Colby College
21 PUBLICATIONS **1,268** CITATIONS
SEE PROFILE

Frank J. Millero
University of Miami
214 PUBLICATIONS **7,477** CITATIONS
SEE PROFILE

Environ. Sci. Technol. 1995, 29, 818–824

Rates and Mechanism of Fe(II) Oxidation at Nanomolar Total Iron Concentrations

D. WHITNEY KING,*,† HEATHER A. LOUNSBURY,† AND FRANK J. MILLERO‡

Department of Chemistry, Colby College, Waterville, Maine 04901, and Rosenstiel School of Marine and Atmospheric Science, University of Miami, 4600 Rickenbacker Causeway, Miami, Florida 33149

A fully automated luminol-based chemiluminescence system has been developed for rapid analysis of Fe(II) at natural levels. Using this system, the rates of Fe(II) oxidation in 0.7 M NaCl have been measured for nanomolar concentrations of Fe(II) over the pH range 7.0–8.3. When the production and decomposition of H_2O_2 in the system were considered, measured rates at these levels were in excellent agreement with a model based on previously reported rate constants determined using micromolar levels of Fe(II). These results show that O_2^- and OH• intermediates produced as a result of Fe(II) oxidation remain effective as Fe(II) oxidants in these controlled conditions. The chemical model for Fe(II) oxidation also allows prediction of steady-state H_2O_2 and O_2^- concentrations that result from the oxidation of micromolar levels of Fe(II). The concentration of both species increases exponentially with increasing pH. At pH 8.2, the predicted H_2O_2 and O_2^- concentrations are 220 and 2.3 nM, respectively. The predicted H_2O_2 concentrations are in excellent agreement with laboratory measurements. These results suggest that significant concentrations of H_2O_2 and O_2^- should be present at the oxic–anoxic interface of marine environments where micromolar levels of Fe(II) are in contact with dissolved oxygen.

Introduction

The redox cycling of iron in marine (*1*, *2*), terrestrial (*3*), and atmospheric (*4*) systems has been an active area of research due to the role this process plays in iron solubility, bioavailability, and oxygen radical chemistry. A critical parameter in these studies is the rate of Fe(II) oxidation. Over the last 30 years, a large number of studies have been made investigating Fe(II) oxidation rates in natural waters (*5–9*). These studies prompted a number of further measurements of the rate of Fe(II) oxidation in well-defined aqueous solutions by both O_2 and H_2O_2 (*10–14*). The proposed mechanism of oxidation is described by reactions 1–4 with reactions 1 and/or 3 being rate limiting:

$$\mathrm{Fe(II)} + \mathrm{O_2} \rightarrow \mathrm{Fe(III)} + \mathrm{O_2^-} \quad (1)$$

$$\mathrm{Fe(II)} + \mathrm{O_2^-} \rightarrow 2\mathrm{H^+} \rightarrow \mathrm{Fe(III)} + \mathrm{H_2O_2} \quad (2)$$

$$\mathrm{Fe(II)} + \mathrm{H_2O_2} \rightarrow \mathrm{Fe(III)} + \mathrm{OH^\bullet} + \mathrm{OH^-} \quad (3)$$

$$\mathrm{Fe(II)} + \mathrm{OH^\bullet} \rightarrow \mathrm{Fe(III)} + \mathrm{OH^-} \quad (4)$$

To date, all systematic studies of Fe(II) oxidation rates have been performed using micromolar Fe(II) solutions. At these high Fe(II) concentrations, a 4:1 stoichiometry of Fe(II) oxidation by oxygen is expected, and a 2:1 stoichiometry of oxidation by hydrogen peroxide has been measured (*11*).

Two outstanding issues are whether the O_2^- and OH• intermediates produced as a result of Fe(II) oxidation remain effective as Fe(II) oxidants at natural Fe(II) (i.e., nanomolar) concentrations where other reduced compounds (e.g., Br^-, Cl^-, CO_3^{2-}) may out compete Fe(II) for O_2^- and OH•, and whether Fe(III) is also in competition for O_2^-:

$$\mathrm{Fe(III)} + \mathrm{O_2^-} \rightarrow \mathrm{Fe(II)} + \mathrm{O_2} \quad (5)$$

The ratio of k_5/k_2 is 15 (see Table 1, ref 15), implying that reduction of Fe(III) by O_2^- could be significant under conditions where soluble Fe(III) exceeds 20% of the total iron pool. This condition is met in acidic atmospheric waters, open ocean waters with very low total iron concentrations (*16*), and possibly in estuarine waters containing Fe(III) ligands. In order to utilize laboratory rate data in models for iron redox cycling in natural waters, these issues must be resolved. This is most directly achieved by making Fe(II) oxidation rate measurements using nanomolar levels of total iron. Several analytical techniques have been developed for trace Fe(II) analysis (*17–19*); unfortunately, the analysis time of these methods makes them inopportune for fast kinetic experiments ($\tau < 1$ min).

Recently, a stopped-flow chemiluminescence system based on the Fe(II)-catalyzed reaction between luminol and oxygen (*20*, *21*) has been optimized for seawater media (*22*). This technique allows for the selective detection of Fe(II) at nanomolar levels and, unlike previous chemiluminescence methods (*23*, *24*), does not require preconcentration of iron prior to analysis. We have incorporated this chemistry into an automated flow injection analysis

† Colby College.
‡ University of Miami.

0013-936X/95/0929-0818$09.00/0

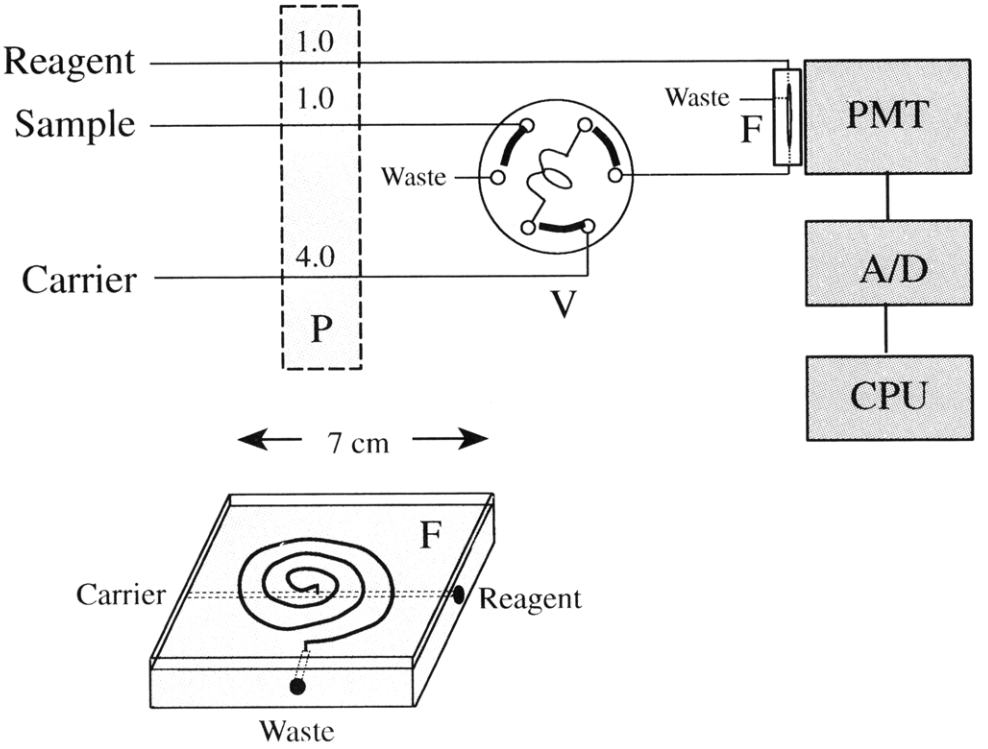

FIGURE 1. Schematic of Fe(II) analysis system with expanded view of flow cell: PMT, integrated photomultiplier tube; A/D, A/D converter and valve controller; CPU, Macintosh computer; P, pump with flow rates listed in mL/min; V, injection valve; F, flow cell.

system which allows rapid, sub-nanomolar detection of Fe(II) in natural waters.

Using this new analytical capability, the oxidation rates of Fe(II) at nanomolar iron concentrations in NaCl media and over a range of pH have been investigated. The results have been used to evaluate a kinetic model for Fe(II) oxidation based on published Fe(II) oxidation reactions and rates. The chemical model for Fe(II) oxidation also allows prediction of steady-state H_2O_2 and O_2^- concentrations that result from Fe(II) oxidation. Measurements of H_2O_2 concentrations have been used to further validate the model.

Experimental Section

Reagents. All solutions were prepared using 0.2 μm filtered, 18.3 MΩ NANOpure water. Hydrogen peroxide (30%), peroxidase (type VI from horseradish), catalase (from bovine liver), *p*-hydroxyphenylacetic acid (POHPAA), tris(hydroxymethyl)aminomethane, and 5-amino-2,3-dihydro-1,4-phthalazinedione (luminol) were obtained from Sigma. All other chemicals were reagent grade and used without purification.

Sodium chloride carrier (0.7 M, pH 7) was prepared at least 24 h in advance to allow for the oxidation of trace Fe(II) impurities (<10 nM) present in the salt. Tris buffers were 0.01 M in 0.7 M NaCl. Hydrogen peroxide standards were made from 30% H_2O_2 standardized by iodometry. The H_2O_2 fluorometric reagent was prepared daily and consisted of 0.25 M Tris buffer (pH 8.3), 0.25 mM POHPAA, and 66 ppm (w/v) peroxidase. Luminol reagent (0.5 mM) was prepared in 0.2 M borate buffer and adjusted to a pH of 10.2 with sodium hydroxide. This reagent was prepared a minimum of 24 h in advance to allow for the slow removal of trace metal impurities from the alkaline reagent due to adsorption onto the walls of the reagent bottle. Stock iron(II) solutions (4 mM) were prepared by dissolving ferrous ammonium sulfate in 0.2 M HCl. Fe(II) standards were prepared daily in a NaCl matrix (0.7 M) adjusted to a pH of 3.0 to prevent oxidation of Fe(II).

Methods. Oxygen concentrations were determined using an automated Winkler titration system with spectrophotometric end point detection. A correction was made to the titration stoichiometry to account for the reduction of thiosulfate to hyposulfate by Fe(III). The pH measurements were made on the free hydrogen ion scale using Tris buffers, an Orion Ross Sure-flow combination electrode, and an Orion meter. Hydrogen peroxide analysis was performed using the method of Miller and Kester (*25*) utilizing a Perkin-Elmer 650-10S fluorescence spectrophotometer.

Fe(II) Analysis. Figure 1 is a schematic of the analysis system. Fe(II) samples were introduced into the luminescence flow cell in a sodium chloride carrier and mixed with a buffered luminol reagent. At pH 10, Fe(II) is oxidized by oxygen on a millisecond time scale catalyzing the oxidation of luminol and producing 426 nm of light. All solutions were delivered with a Rainin Rabbit Plus peristaltic pump using Tygon or Vitron pump tubing. All other tubing was Teflon with polypropylene fittings. A Valco Inc. automated six-way injection valve with a pneumatic actuator was used for sample injection.

The flow cell consisted of a spiral T-cell made of Plexiglas that was situated directly in front of a Hamamatsu 124-06 integrated photomultiplier tube. The detector employed a R268 PMT with a 1 MW transimpedance wide band amplifier and an internal Cockroft-Walton high-voltage multiplier.

The PMT voltage signal was recorded using a DGH Corporation Model D1141 15-bit, 8-Hz analog to digital converter. Two logic signals from the DGH module were used to control the injection valve. The DGH module was controlled via RS 232 communication by a Macintosh SE/30 microcomputer.

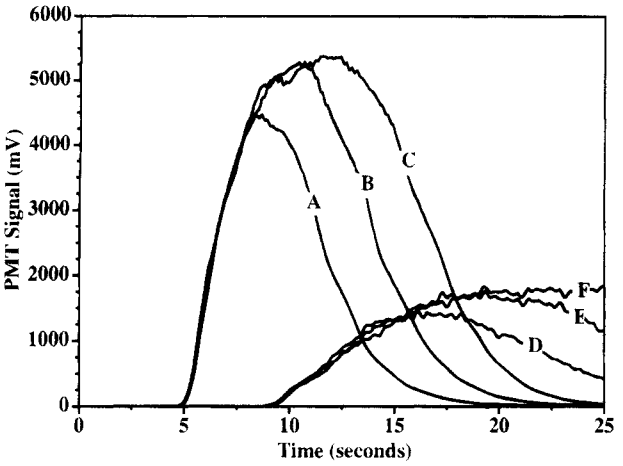

FIGURE 2. System response using a 100 nM Fe(II) sample as a function of flow rate and injection loop volume. Curves A–C are for 5 mL/min flow rate and 200, 400, and 800 μL loop volume, respectively. Curves D–F are for 2.5 mL/min flow rate and 200, 400, and 800 μL loop volume, respectively.

Optimization of Fe(II) System. Figure 2 shows the response of the FIA system over a range of solution flow rates and injection loop volumes. Maximum signals were obtained with a sample loop volume greater than 700 μL. Signals continued to increase with increasing flow rate, consistent with the very rapid Fe(II)–oxygen–luminol reaction rate. An operating flow rate of 5 mL/min was selected as a compromise between signal intensity, tubing integrity, and reagent consumption rate.

As the luminol reagent aged for several days, the signal intensity of the system increased by as much as 100%, a probable result of slow removal of trace metal impurities from the alkaline reagent due to adsorption onto the walls of the reagent bottle. System sensitivity was adjusted by regulating the PMT high voltage to achieve maximum signal to noise for a selected Fe(II) concentration range. Figure 3 shows standard curves over two concentration ranges. The system response was linear over an order of magnitude Fe(II) concentration range. Over larger concentration ranges, a well-characterized curve was obtained. The curvature is probably a result of trace metal impurities in the luminol and NaCl reagents. Later work has confirmed that passing the luminol reagent through an 8-hydroxyquinoline column results in linear standard curves and eliminates the aging effect observed for the luminol reagent. The system response was insensitive to changes in sample H_2O_2, and Fe(III) concentrations over the H_2O_2 and Fe(III) ranges from 0 to 1 μM. Standards of appropriate Fe(II) concentrations were used to characterize the system response curve before each experiment.

Oxidation Experiments. Fe(II) oxidation experiments were performed by adding 300 nM Fe(II) to the O_2-saturated 0.7 M NaCl solutions buffered with 0.009 M HCO_3^-. The solutions were contained in a 500-mL Pyrex water-jacketed beaker fitted with a Lucite top. Solution temperatures were maintained at 25.0 ± 0.1 °C using a Neslab RTE-220 thermocirculator. Fe(II) concentrations were measured every 60 s over the duration of each experiment. H_2O_2 concentrations were measured at the beginning of each kinetic run.

In a separate set of experiments, the steady-state concentration of H_2O_2 produced as a result of Fe(II) oxidation was determined. A range of solutions (0.7 M NaCl, 0.009 M $NaHCO_3$) were adjusted with HCl or NaOH to a pH between 6 and 8.5. The solutions were brought to 25.0 °C in a thermocirculator, injected with Fe(II) (1–10 μM), and allowed to stand until 99% of the Fe(II) had been oxidized. Each solution was then analyzed for H_2O_2. The maximum reaction time for Fe(II) oxidation was 12 h. In these clean, abiotic solutions, the loss of H_2O_2 by pathways other than reduction by Fe(II) was minor.

Numerical Model. The Fe(II) oxidation kinetics were modeled using the kinetics package Stella running on a Macintosh SE/30 microcomputer. The solutions were based on fourth order Runge Kutta approximations with appropriate time step. The model accounted for Fe(II), O_2, O_2^-, H_2O_2, and OH• reactions and rates (corrected for pH) in order to predict the overall rate of Fe(II) oxidation.

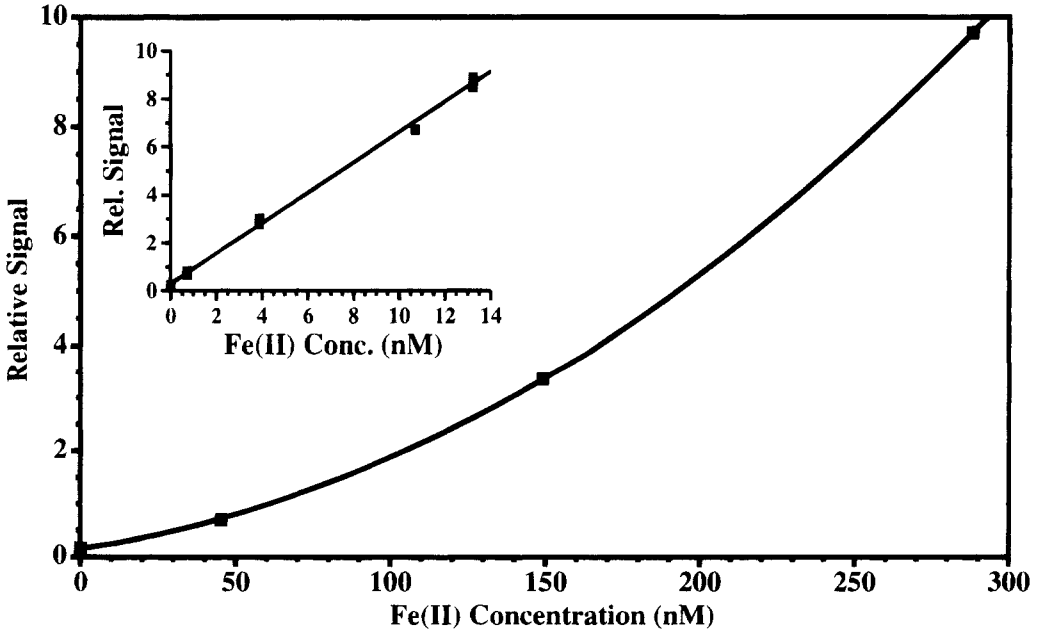

FIGURE 3. System response as a function of added Fe(II). System sensitivity was adjusted by regulating the PMT high voltage to 650 V 0–300 nM Fe(II) and 1000 V 0–15 nM Fe(II); the flow rate was 5 mL/min; and the injection loop volume was 700 μm.

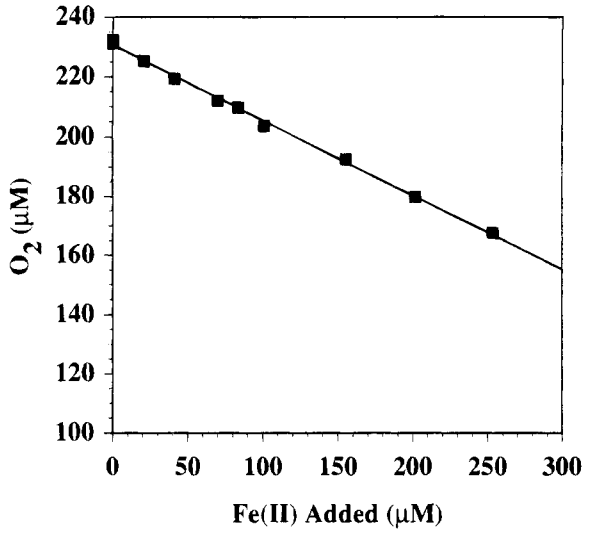

FIGURE 4. Oxygen concentration after complete oxidation of Fe(II) in 35‰ seawater as a function of added Fe(II).

Results and Discussion

Figure 4 is a plot of final O_2 concentration as a function of Fe(II) added at micromolar levels to a series of 35‰ seawater samples at pH 8.0. The slope of the line is, 0.251 ± 0.004, which is in agreement with the predicted stoichiometry of 4:1, and confirms the assumed stoichiometry reported in numerous studies of Fe(II) oxidation using high initial Fe(II) concentrations (*5, 10, 12, 26*).

A first-order plot of Fe(II) oxidation using 300 nM initial Fe(II) is shown in Figure 5. Due to the significant curvature in the plot of log[Fe(II)] versus time, a first-order rate expression cannot be obtained from this data for the full time course of the experiment. The rate of Fe(II) oxidation increases as Fe(II) concentrations decrease. The oxidation of Fe(II) is autocatalytic, but only for total iron concentrations above 50 μM (*8*) or total iron concentrations 100 times higher than the levels used in these experiments. Instead,

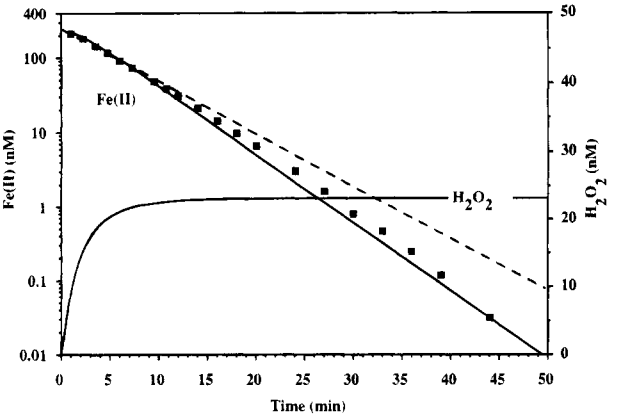

FIGURE 5. Actual and modeled Fe(II) and H_2O_2 concentrations as a function of time in 0.7 M NaCl, pH 7.5, at 25.0 °C. Symbols are for experimental data. Solid lines are for Fe(II) and H_2O_2 model fits, and the dashed line is the initial rate of Fe(II) oxidation.

the data is consistent with two homogeneous rate-limiting steps for Fe(II) oxidation; Fe(II) oxidation by O_2 (eq 1) and Fe(II) oxidation by H_2O_2 (eq 3). Assuming reactions 2 and 4 are fast and stoichiometric with respect to Fe(II), the rate of change of Fe(II) and H_2O_2 is described by eqs 6 and 7, respectively.

$$d\text{Fe(II)}/dt = -2k_1[\text{Fe(II)}][O_2] - 2k_3[\text{Fe(II)}][H_2O_2] \quad (6)$$

$$dH_2O_2/dt = k_1[\text{Fe(II)}][O_2] - k_3[\text{Fe(II)}][H_2O_2] \quad (7)$$

Values for the rate constants as a function of pH are listed in Table 1. Figure 5 also shows the predicted Fe(II) concentrations calculated using a model that incorporates both H_2O_2 production and consumption. Over the Fe(II) concentration range 300–0.3 nM, experimental and modeled concentrations are in excellent agreement. The model predicts the formation of 22 nM H_2O_2. The rate of Fe(II) oxidation becomes pseudo-first-order once the steady-state levels of H_2O_2 are reached. The curvature in the log[Fe(II)]

TABLE 1

Reactions and Rate Constants for Fe(III), Fe(II), and OH• in Aqueous Solution (0.7 M NaCl, 0.009 M $NaHCO_3$)[a] at 25.0 °C

no.	reaction	k (M^{-1} s^{-1})	ref[b]
1	$Fe(II) + O_2 \rightarrow Fe(III) + O_2^-$	$\log(k) = -13.77 + 2.0$ (pH) $\log(K') = 13.65$[c]	1
2	$Fe(II) + O_2^- \rightarrow 2H^+ \rightarrow Fe(III) + H_2O_2$	1.0×10^7	2
3	$Fe(II) + H_2O_2 \rightarrow Fe(III) + OH^\bullet + OH^-$	$\log(k) = -2.45 + 0.972$ (pH) $\log(K') = 11.08$[c]	3
4	$Fe(II) + OH^\bullet \rightarrow Fe(III) + OH^-$	5.0×10^8	4
5	$Fe(III) + O_2^- \rightarrow Fe(II) + O_2$	1.5×10^8	2
8	$OH^\bullet + Cl^- \rightarrow HOCl^-$	4.3×10^9 6.1×10^9	5 (rev)[d] 5
9	$HOCl^- + H^+ \rightarrow Cl^\bullet + H_2O$	2.1×10^{10} 1.3×10^3	5 (rev) 5
10	$Cl^\bullet + Cl^- \rightarrow Cl_2^-$	2.1×10^{10} 1.1×10^5	5 (rev) 5
11	$Cl_2^- + Cl_2^- \rightarrow Cl_3^- + Cl^-$	3.1×10^9	5
12	$Cl_3^- = Cl_2 + Cl^-$	0.18[e]	5
11	$Cl_2^- + Fe^{2+} \rightarrow Fe^{3+} + 2Cl^-$	1.0×10^7	6
14	$OH^\bullet + HCO_3^- \rightarrow H_2O + CO_3^{-\bullet}$	1.5×10^7	7
15	$OH^\bullet + CO_3^{2-} \rightarrow OH^- + CO_3^-$	4.2×10^8	7
16	$O_2^- + O_2^- \rightarrow 2H^+ \rightarrow H_2O_2 + O_2$	$\log(k) = 12.7 - 1.0$ (pH)	8

[a] The rate constants for reactions 1 and 4 are apparent constants corrected for ionic strength, media composition, and pH (free scale). All other rate constants are for aqueous solutions without corrections for media effects. [b] References: (1) ref 12, valid over the pH range 6.0–8.3, the rate for reaction 1 is calculated from the reported rate, k_{O_2} ($k = 0.25k_{O_2}$); (2) ref 15, for soluble iron species at pH > 6; (3) ref 13, valid over the pH range 6.0–8.0, the rate for reaction 4 is calculated from the reported rate, $k_{H_2O_2}$ ($k = 0.5k_{H_2O_2}$); (4) ref 27; (5) ref 28; (6) ref 29; (7) ref 30; (8) ref 31, valid for pH > 6. [c] Overall rate as defined by eq 16. [d] Rate for reverse reaction (rev). [e] (K M^{-1}).

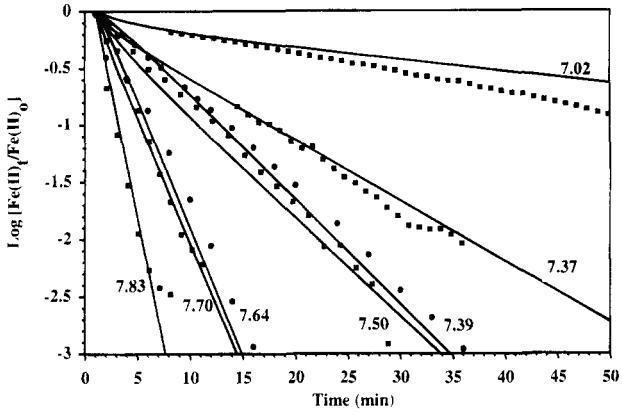

FIGURE 6. Actual and modeled Fe(II) concentrations as a function of time for solutions with a range of pH in 0.7 M NaCl at 25.0 °C. Initial Fe(II) concentration was 300 nM. Symbols are for experimental data, and solid lines are for model fits.

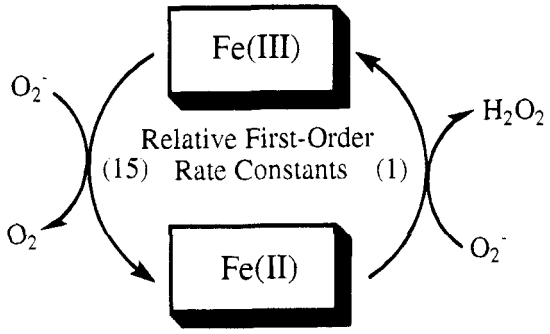

FIGURE 7. Iron-catalyzed disproportionation of O_2^-. Absolute rates for the forward (eq 3) and reverse (eq 2) reactions are reported in Table 1.

versus time has not been observed in previous studies because the micromolar levels of Fe(II) used produces steady-state levels of H_2O_2 within a few seconds.

Figure 6 shows experimental and modeled log[Fe(II)] versus time plots for solutions having different pH. Generally, the agreement between experimental and modeled rate data is very good. In all experiments, accurate measurement of the initial H_2O_2 concentration was critical because solutions exposed to laboratory air often have H_2O_2 concentrations above 50 nM. The poor agreement of the data with the model at pH 7.0 may be due to contamination of the solution with atmospheric H_2O_2 over the course of the oxidation experiment.

The agreement between modeled Fe(II) oxidation rates and observed rates suggests that in these clean NaCl solutions, reactions 2 and 4 are fast and stoichiometric even at low nanomolar levels of Fe(II). In the case of the O_2^- reaction (eq 2), this is not unexpected since the rate of O_2^- reaction with only 1 nM of Fe(II) will exceed the O_2^- disproportionation rate (eq 15, Table 1) by a factor of 300. The back-reaction of Fe(III) with O_2^- might be expected to occur as the concentration of Fe(II) approaches the solubility limit of Fe(III). Under these conditions, the disproportionation of O_2^- is catalyzed by an iron redox cycle, which will result in no net oxidation of Fe(II) (Figure 7).

The occurrence of this cycle in acid rain water has been demonstrated by Sedlak and Hoigné (*32*). No evidence of the cycle is found in these studies since the rate of Fe(II) oxidation did not decrease at low Fe(II) concentrations (Figure 6). This could be due to several reasons. One, the Fe(III) is insoluble. Estimates of the solubility of hydrous ferric oxide {$Fe(OH)_3(s)$} in our solutions at pH 8 range from 2 to 0.07 nM (*16, 33*). However, these estimates are probably low due to the slow rate of $Fe(OH)_3(s)$ formation relative to Fe(II) oxidation. Two, by the time Fe(II) concentrations are less than 1.5 nM, the H_2O_2 concentrations are at least 15 nM. This 10-fold excess of H_2O_2 will maintain oxidation rates of at least 50% of the maximum rate (e.g., where reactions 1 and 3 are rate limiting). Some of our results show a reduction in oxidation rate below 1 nM, but quantifying the rate change at Fe(II) concentrations near the detection limit of the analytical system is unrealistic. A more sensitive approach for evaluating the Fe(II) cycle may be to measure the steady-state O_2^- concentration.

The experimental data support the stoichiometric oxidation of Fe(II) by OH•. However, analysis of competing OH• reduction pathways indicates that the oxidation of Fe(II) by OH• in these experiments must be occurring via a radical intermediate. Both Cl^- and carbonate (CO_3^{2-} and HCO_3^-) will out compete Fe(II) for OH•. A numerical model incorporating Fe(II) oxidation (eq 4), Cl^- oxidation (eqs 8–13), and carbonate oxidation (eqs 14 and 15) predicts that less than 1% of the OH• is reduced directly by Fe(II).

$$OH^\bullet + Cl^- \rightarrow HOCl^- \quad (8)$$

$$HOCl^- + H^+ \rightarrow Cl^\bullet + H_2O \quad (9)$$

$$Cl^\bullet + Cl^- \rightarrow Cl_2^- \quad (10)$$

$$Cl_2^- + Cl_2^- \rightarrow Cl_3^- + Cl^- \quad (11)$$

$$Cl_3^- = Cl_2 + Cl^- \quad (12)$$

$$Cl_2^- + Fe^{2+} \rightarrow Fe^{3+} + 2Cl^- \quad (13)$$

$$OH^\bullet + HCO_3^- \rightarrow H_2O + CO_3^- \quad (14)$$

$$OH^\bullet + CO_3^{2-} \rightarrow OH^- + CO_3^- \quad (15)$$

The most significant OH• reduction pathway is the reaction with HCO_3^- at solution pH below 7.8 and CO_3^{2-} above pH 7.8. The observed 4:1 Fe(II)/O_2 stoichiometry (Figure 4) implies that the CO_3^- radical must be involved in Fe(II) oxidation by acting as an intermediate in the oxidation of Fe(II) by •OH. The high Fe(II) concentrations used in the Fe(II)/O_2 stoichiometry calculations do not compromise this conclusion, since even at 100 μm Fe(II) 99% of the OH• should react with CO_3^{2-}.

An independent test of the oxidation model for Fe(II) is the measurement of the concentration of H_2O_2 and O_2^- produced as intermediates of oxidation. The rates of production and consumption of H_2O_2 due to Fe(II) oxidation are described by reactions 1 and 3, respectively, and are equal under steady-state conditions.

$$@ \text{ steady state } dH_2O_2/dt = 0 = k_1[Fe(II)][O_2] - k_3[Fe(II)][H_2O_2] \quad (16)$$

The rates of reactions 1 and 3 are strongly pH dependent, with the OH^- dependencies being second and first order, respectively (*12, 34*). Incorporating these dependencies into eq 16 and solving for H_2O_2 yields an expression describing the steady-state H_2O_2 concentration as a function of OH^-.

$$k_1'[\text{Fe(II)}][O_2]\,[OH^-]^2 = k_3'[\text{Fe(II)}][H_2O_2][OH^-] \quad (17)$$

$$[H_2O_2] = \frac{k_1[\text{Fe(II)}][O_2]}{k_3[\text{Fe(II)}]} = \frac{k_1'[OH^-][O_2]}{k_3'} \quad (18)$$

Predicted H_2O_2 concentrations are compared to observed concentrations in Figure 8. All H_2O_2 data are within 1 standard deviation of the predicted values based on the uncertainty of the published values for k_1' and k_3'. The slope of the experimental data ($0.96 \pm 0.04 \times 10^8$) is also consistent with the slope of the modeled data ($0.54 \times 10^8 - 1.2 \times 10^8$).

A similar analysis can be performed for O_2^-. The steady-state solution for O_2^- production and consumption by Fe(II) oxidation is described by

$$dO_2^-/dt = 0 = k_1[\text{Fe(II)}][O_2] - k_2[\text{Fe(II)}][O_2^-] \quad (19)$$

where rearrangement yields the steady-state O_2^- concentration:

$$[O_2^-] = \frac{k_1[\text{Fe(II)}][O_2]}{k_2[\text{Fe(II)}]} = \frac{k_1'[OH^-]^2[O_2]}{k_2} \quad (20)$$

The predicted steady-state O_2^- concentration (Figure 9) exhibits an exponential increase as a function of pH due to the $(OH^-)^2$ dependencies (eq 20). At pH 8.2, the predicted steady-state concentration should reach 2 nM. While we have not made measurements of O_2^-, this concentration should be detectable using the NO-based analytical techniques of Zafiriou and co-workers (*35, 36*).

The success of the kinetic model at predicting Fe(II) oxidation rates and the ability of the model to predict intermediate concentrations demonstrate the validity of the kinetic model for Fe(II). Confirming that apparent rate constants for Fe(II) oxidation measured using micromolar Fe(II) concentrations can be interpreted in the context of the elementary redox reactions (eqs 1–4). These elementary reactions and rates are appropriate for modeling Fe(II) oxidation at nanomolar concentrations. While we have focused on NaCl solutions, the kinetic model should be applicable to a wide range of natural waters, including seawater, if the effect of ionic strength, media, and temperature are accounted for in the rate constants. The effect of these parameters on oxidation rates have been extensively measured by Millero and his co-workers (*10, 12, 13, 37*).

A limitation of any kinetic model for Fe(II) oxidation is the uncertainty in the role organic ligands will play in the Fe(II) oxidation rates. Fe(II)–organic complexes can both accelerate and decelerate Fe(II) oxidation rates (*7, 10, 32, 38*). At nanomolar levels of iron, the fraction of Fe(II) complexed by organic ligands could be significant. The effect of organics will be most pronounced in lake and estuarine systems where dissolved organic carbon concentrations are high. Future work will need to reconcile the oxidation rate of Fe(II) in organic-rich natural waters with laboratory measurements of Fe(II) oxidation in media containing model organic compounds.

In the surface waters of alkaline lakes and the ocean, the concentration of Fe(II) is below 20 nM. Due to the low Fe(II) concentration, the direct oxidation of Fe(II) will not be a significant source of H_2O_2 or O_2^- to these waters. However, the photoreduction of Fe(III) does provide a

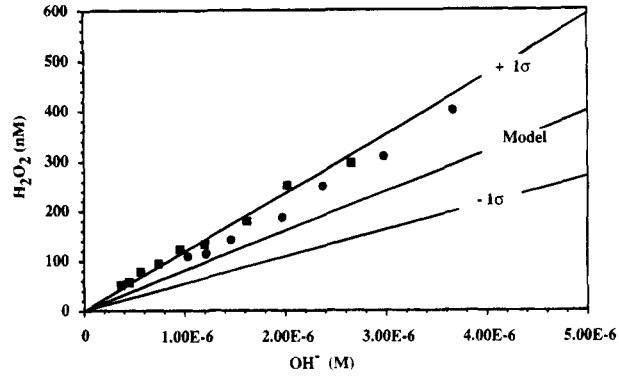

FIGURE 8. Actual and modeled steady-state H_2O_2 concentrations as a function of OH^- concentration resulting from Fe(II) oxidation in 0.7 M NaCl at 25.0 °C. Symbols are for experimental data obtained after a 1 μM Fe(II) addition and 2-h oxidation (●) and 10 μM Fe(II) addition and 10-h oxidation (■). The solid lines are for model fits with propagated uncertainties.

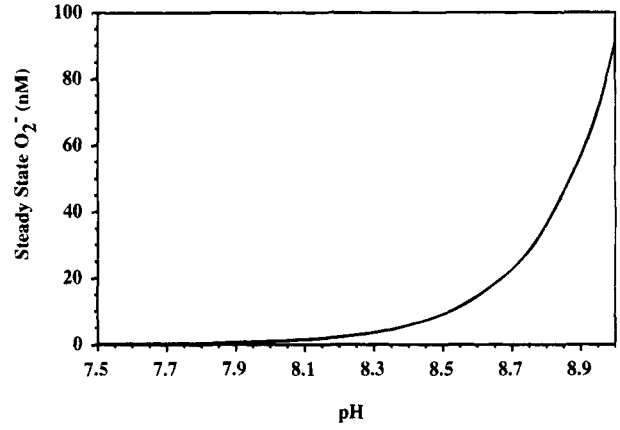

FIGURE 9. Predicted O_2^- steady-state concentration as a function of pH resulting from Fe(II) oxidation.

potential mechanism for producing Fe(II) and H_2O_2 (*4, 39*). It is the time-integrated flux of Fe(II) in the system not the steady-state concentration that will determine H_2O_2 concentrations (eq 18). The rate of photoreduction of inorganic Fe(III) species is very slow above a pH of 7 (*1*), while organic Fe(III) complexes such at Fe(III)–citrate or Fe(III)–oxalate are highly photochemically active (*4, 39*). The rate of Fe(II) production due to Fe(III)–citrate photoreduction by 350–450 nm of sunlight is

$$k' = 2.303I(\phi\epsilon)L \quad (21)$$

$$d\text{Fe(II)}/dt = k'[\text{Fe(III)–citrate}] \quad (22)$$

where I is the wavelength and volume-averaged incident light intensity for surface seawater (2.8×10^{-4} Einstein L^{-1} min^{-1}, 350–450 nm, midday summer solar photon flux at 40° N latitude), ϕ is the wavelength-averaged quantum yield (ϕ = 0.25 (*40*)), ϵ is the wavelength-averaged molar absorptivity ($\epsilon = 500\ M^{-1}\ cm^{-1}$ (*41*)), and L is the pathlength (10 cm). The calculated rate, k', is 0.8 min^{-1}, which is in agreement with the value calculated by Faust and Zepp (*40*). Using the approach described by King et al. (*1*) and a total iron concentration of 20 nM (coastal waters), this photoreduction rate predicts a steady-state Fe(II) concentration of 8 nM, a Fe(II) turnover rate of 29 h^{-1}, and an integrated Fe(II) flux of 230 nM/h for surface waters. The predicted steady-state concentrations of H_2O_2 and O_2^- in seawater at pH 8.0 are 46 and 0.42 nM, respectively. Mass

balance constraints require 140 nM of Fe(II) to produce 46 nM of H_2O_2, indicating that steady-state H_2O_2 concentrations could be reached after 0.6 h of Fe(III)–citrate photolysis. Steady-state concentrations of O_2^- would easily be reached in this time. The oxidized organic chromophore will also react with O_2 to form O_2^- and then H_2O_2 (*40*).

These calculations represent upper limits of H_2O_2 and O_2^- production by iron redox cycling. The concentration and photoreactivity of Fe(III)–organic complexes are poorly characterized and may have a slow formation rate relative to the iron turnover rate. As mentioned previously, any Fe(II)–organic complexes formed may have very different oxidation rates. Finally, direct photolysis of natural organic matter is expected to dominate O_2^- and H_2O_2 production in natural waters (*42*). Therefore, iron photoredox cycling is most likely a minor pathway for O_2^- and H_2O_2 production in surface waters.

However, at oxic–anoxic interfaces, the production of O_2^- and H_2O_2 by Fe(II) oxidation could be significant. Fe(II) concentrations in the anoxic pore waters and deep waters of lakes and the ocean often exceed 1 μM. At the oxic–anoxic interface, Fe(II) will be oxidized by dissolved oxygen producing both O_2^- and H_2O_2. Thus, redox cycling of iron at the interface will not be necessary to produce these predicted steady-state concentrations. To date, no field measurements of O_2^- or H_2O_2 at an oxic–anoxic interface have been made since field studies have been concentrated on the photochemical production of these species. We expect the actual concentration of O_2^- and H_2O_2 just above the interface to be a function of several variables: oxygen concentration, steepness of the chemical gradient, and concentration of other reduced species. Rapid reactions of both O_2^- and H_2O_2 with reduced sulfur or manganese will lower observed O_2^- and H_2O_2 concentrations.

In conclusion, a new analytical system has been developed to measure Fe(II) oxidation rates using total iron concentrations typical of natural systems. When the production and decomposition of H_2O_2 in the system were considered, measured rates at these levels were in excellent agreement with a model based on previously reported rate constants. These results confirm that apparent rate constants for Fe(II) oxidation measured using micromolar Fe(II) concentrations can be interpreted in the context of the elementary redox reactions and that these rates can be used for kinetic models of Fe(II) oxidation provided the effect of ionic strength, media, and temperature are taken into account. An interesting result of the modeling efforts of Fe(II) oxidation is the prediction of high steady-state concentrations O_2^- and H_2O_2 produced as intermediates on Fe(II) oxidation. In the case of H_2O_2, the model results have been confirmed experimentally. Future field sampling is needed to establish the importance of Fe(II) redox cycling in the production of H_2O_2 under conditions of variable organic carbon, sulfur, and metal concentrations.

Acknowledgments

This work was supported by a William and Flora Hewlett Foundation Award of the Research Corporation to D.W.K., a Clare Boothe Luce research assistantship for H.A.L., and grants from the Oceanographic section of NSF and ONR to F.J.M. We thank Dan O'Sullivan for helpful discussions concerning the Fe(II) analysis system.

Literature Cited

(1) King, D. W.; Aldrich, R. A.; Charnecki, S. E. *Mar. Chem.* **1993**, *44*, 105–120.
(2) Miller, W. L. An Investigation of Peroxide, Iron and Iron Bioavailability in Irradiated Marine Waters. Thesis, University of Rhode Island, 1990.
(3) McKnight, D. M.; Kimball, B. A.; Bencala, K. E. *Science* **1988**, *240*, 637–640.
(4) Zuo, Y.; Hoigné, J. *Environ. Sci. Technol.* **1992**, *26*, 1014–1022.
(5) Stumm, W.; Lee, G. F. *Ind. Eng. Chem.* **1961**, *53*, 143–146.
(6) Sung, W.; Morgan, J. J. *Environ. Sci. Technol.* **1980**, *14*, 561–568.
(7) Theis, T. L.; Singer, P. C. *Environ. Sci. Technol.* **1974**, *8*, 569–573.
(8) Tamura, H.; Goto, K.; Nagayama, M. *Corros. Sci.* **1976**, *16*, 197–207.
(9) Davidson, W.; Seed, G. *Geochim. Cosmochim. Acta* **1983**, *47*, 67–79.
(10) Millero, F. J.; Sotolongo, S.; Izaguirre, M. *Geochim. Cosmochim. Acta* **1987**, *51*, 793–801.
(11) Millero, F. J.; Sotolongo, S. *Geochim. Cosmochim. Acta* **1989**, *53*, 1867–1873.
(12) Millero, F. J.; Izaguirre, M. *J. Solution Chem.* **1989**, *18*, 585–599.
(13) Millero, F. J.; Sotolongo, S.; Stade, D. J.; Vega, C. A. *J. Solution Chem.* **1991**, *20*, 1079–1092.
(14) Moffett, J. W.; Zika, R. G. *Environ. Sci. Technol.* **1987**, *21* (8), 804–810.
(15) Rush, J. D.; Bielski, B. H. J. *J. Phys. Chem.* **1985**, *89*, 5062–6.
(16) Zhu, X.; Prospero, J. M.; Millero, F. J.; Savoie, D. L.; Brass, G. W. *Mar. Chem.* **1992**, *38*, 91–107.
(17) King, D. W.; Lin, L.; Kester, D. R. *Anal. Chim. Acta* **1991**, *247*, 125–132.
(18) Hong, H.; Kester, D. R. *Limnol. Oceanorg.* **1986**, *31* (3), 512–524.
(19) Waite, T. D.; Morel, F. M. M. *Anal. Chem.* **1984**, *56* (4), 787–92.
(20) Seitz, W. R.; Hercules, D. M. *Anal. Chem.* **1972**, *44*, 2143–2149.
(21) Klopf, L. L.; Nieman, T. A. *Anal. Chem.* **1983**, *55*, 1080–1083.
(22) O'Sullivan, D. W.; Hansen, A. K.; Kester, D. R. *Mar. Chem.*, submitted for publication.
(23) Elrod, V. A.; Johnson, K. S.; Coale, K. H. *Anal. Chem.* **1991**, *63*, 893–898.
(24) Obata, H.; Karatani, H.; Nakayama, E. *Anal. Chem.* **1993**, *65*, 1524–1528.
(25) Miller, W. L.; Kester, D. R. *Anal. Chem.* **1988**, *60*, 2711–2715.
(26) Kester, D. R.; Byrne, R. H.; Liang, Y.-J. *Marine Chemistry in the Coastal Environment*; ACS Symposium Series 18; American Chemical Society: Washington, DC, 1975; pp 56–79.
(27) Farahataziz; Ross, A. B. *Selected specific rates of reactions of transients from water in aqueous solution, III, Hydroxyl radical and perhydroxyl radical and their radical ions*; Report NRSDS-NBS 59; Washington, DC, 1977; p 113.
(28) McElroy, W. J. *J. Phys. Chem.* **1990**, *94*, 2435–2441.
(29) Thornton, A. T.; Laurence, G. S. *J. Chem. Soc., Dalton Trans.* **1973**, 804–813.
(30) Weeks, J. L.; Rabani, J. *J. Phys. Chem.* **1966**, *70*, 2100–2106.
(31) Zafiriou, O. C. *Mar. Chem.* **1990**, *30*, 31–43.
(32) Sedlak, D. L.; Hoigné, J. *Atmos. Environ.* **1993**, *27A*, 2173–2185.
(33) Byrne, R. H.; Kester, D. R. *Mar. Chem.* **1976**, *4*, 255–274.
(34) Millero, F. J.; Sotolongo, S.; Stade, D. J.; Vega, C. A. *J. Solution Chem.* **1991**, *20*, 1079–92.
(35) Zafiriou, O. C.; Dister, B. *J. Geophys. Res.* **1991**, *96*, 4939–4945.
(36) Micinski, E.; Ball, L. A.; Zafiriou, O. C. *J. Geophys. Res.* **1993**, *98*, 2299–2306.
(37) Millero, F. J. In *Chemical Modeling of Aqueous Systems II*, Melchior, D. C., Bassett, R. L., Eds.; American Chemical Society: Washington, DC, 1990; pp 447–460.
(38) Miles, C. J.; Brezonik, P. L. *Environ. Sci. Technol.* **1981**, *15*, 1089–95.
(39) Zepp, R. G.; Faust, B. C.; Hoigné, J. *Environ. Sci. Technol.* **1992**, *26*, 313–319.
(40) Faust, B. C.; Zepp, R. G. *Environ. Sci. Technol.* **1993**, *27*, 2517–2522.
(41) Timberlake, C. F. *J. Chem. Soc.* **1964**, 5078–5085.
(42) Cooper, W. J.; Zika, R. G.; Petasne, R. G.; Plane, J. M. C. *Environ. Sci. Technol.* **1988**, *22*, 1156–1160.

Received for review November 14, 1994. Accepted November 22, 1994. [⊗]

ES940212U

[⊗] Abstract published in *Advance ACS Abstracts,* January 1, 1995.